Universal laws in the force-induced unraveling of biological bonds

Yuriy V. Pereverzev and Oleg V. Prezhdo
Department of Chemistry, University of Washington, Seattle, Washington 98195-1700, USA
(Received 11 July 2005; revised manuscript received 9 August 2006; published 8 January 2007)

Universal laws in the force-induced unbinding of receptor-ligand complexes are established for a general functional dependence of the dissociation rate constant on the applied force and are detailed with the two-pathway model that describes the recently discovered biological catch bond. The relationships link the data obtained with constant and time-dependent forces in different regimes, provide common representation for the previously unrelated data sets, and, thereby, greatly facilitate analysis and interpretation of experiments. The universal laws are demonstrated with the monomeric and dimeric catch-slip bonds between P-selectins and P-selectin glycoprotein ligands-1, and the slip bond between E-selectin and sialyl Lewis^x antigen.

DOI: 10.1103/PhysRevE.75.011905 PACS number(s): 87.15.La, 05.70.Ln, 87.15.Aa, 87.64.Dz

I. INTRODUCTION

Biological adhesion shows a great variety of binding motifs that are optimized for specific life functions. Often, biological adhesion operates under force, such as in the binding of leukocytes to blood vessel walls that occurs via selectin receptors and is optimized to function under shear blood flow [1–5]. Macromolecular binding forces between individual protein-ligand pairs are measured directly with atomic force microscopy and optical tweezers, revealing many surprising and formerly hidden adhesion properties that cannot be detected by studies of near equilibrium dissociation [6]. The range of the studied phenomena extends from mechanical properties and unzipping of DNA [7,8], to protein folding, unfolding [9,10], and crystallization [11], to friction through dynamical formation and rupture of molecular bonds [12]. The discovery of the counterintuitive adhesion strengthening under a separating force in the receptor-ligand complexes between P-, L-selectins and P-selectin glycoprotein lidand-1 (PSGL-1) [1–5], as well as fimbria protein type H (FimH) and mannose [13,14], constitutes a particularly intriguing example. This type of receptor-ligand interaction has been named "catch-binding" [15], in contrast to the typical "slip-binding," where adhesion weakens with force [6,16–19].

Accurate interpretation of these and numerous related experiments is critical for understanding of biological adhesion and requires proper representation of the data. Experimental uncertainties and multiple components that are present in biological systems and are often hard to control with sufficient reliability create considerable challenges for data analysis. Results are often very sensitive to details of experimental setup and vary between laboratories and, sometimes, even between different runs in the same experiment. As a result, suitable data representation becomes a key to the analysis.

The current article derives universal laws that establish profound relationships between the experiments carried out under different conditions. These universal laws provide common representation for the previously unrelated data sets, and allow one to detect and investigate discrepancies that can lead to better experiments and, ultimately, new discoveries. The derived relationships create internal consistency tests for the commonly used models, improve the quality of fits, and reduce error bars on system parameters. The universal laws equip experimentalists with guidelines for systematically varying experimental parameters, such as magnitudes of constant forces, jump forces, and ramp rates.

The relationships established below are presented in a mathematical form that places the experimental observables on one side of the equation and the physical characteristics that follow from a specific model on the other side. This mathematical form gives universal data representations that are independent of the model, and provides the basis for testing of different models against the same experimental quantities. The observables that depend on multiple variables are mapped onto functions of fewer variables, simplifying the analysis and creating links between different data sets, for instance, those obtained in constant and time-dependent force regimes or different time-dependent regimes.

We start by establishing the general universal laws that follow from the mathematical form of kinetic equations describing bond dissociation. The analysis continues assuming the simple exponential dependence of the dissociation rate constant on the applied force. The assumption, introduced by Bell [16], is used in the overwhelming majority of publications in the field, leading to the detailed universal relationships that can be expected to find wide applicability with the current experiments. The relationships are formulated for both bond-survival probability and probability density, which are commonly used to represent the data. In addition to the distribution function maxima that achieved the primary focus in most publications, we investigate other properties of the distributions, such as its width and asymmetry. Particular attention is paid to the now-standard constant-force and jump-ramp experimental protocols. The derived relationships are illustrated with the catch-slip bond, which presents a particularly interesting case of biological adhesion, whereby a force attempting to break the bond makes it stronger. The ordinary slip bond is considered separately as a limit of the catch-slip bond.

II. GENERAL UNIVERSAL RELATIONSHIPS

A number of universal relationships follow from the simple form of the kinetic equation for the bond-survival probability $P(t)$ that underlies the most-familiar models used

to describe biological binding and force-induced unbinding [6,20–24]:

$$\frac{dP(t)}{dt} = -\nu(f)P(t). \quad (1)$$

Here $\nu(f)$ is the Kramer's transition rate for the escape of a ligand from a receptor binding pocket. In the pulling-force experiments the rate depends on the force f that, generally, is a function of time t. In cases where the force is time independent, the inverse of the rate $1/\nu(f)$ is equal to the average lifetime of the ligand in the bound state.

Equation (1) is valid for the simple slip bond, where the potential energy profile describing the receptor-ligand interaction contains a single bound-state minimum and a finite barrier for the escape from the bound state [16–19]. Equation (1) also holds for a more complex potential profile comprised of a deep minimum and a series of shallow intermediate minima, in which case the rate of unbinding becomes the sum of times of transit over individual barriers starting from the deepest minimum [6]:

$$\nu(f)^{-1} = \sum_i \nu_i(f)^{-1}. \quad (2)$$

Equation (1) also describes the catch-slip bond that was first predicted theoretically [15] and later discovered experimentally [1–5,13,14] and modeled [22–24] with the dissociation rate

$$\nu(f) = k_{1s}(f) + k_{1c}(f) \quad (3)$$

comprised of the contributions from the catch (c) and slip (s) pathways.

A. Probability and probability-density

The formal solution of Eq. (1) is

$$P(t) = \exp\left[-\int_0^t \nu(f)dt'\right]. \quad (4)$$

In the important special case of the time-independent force [3,4,7–9] it immediately follows that

$$-\frac{\ln P(f,t)}{t} = \nu(f), \quad (5)$$

mapping the original experimentally observed $P(f,t)$ that depends on f and t onto a function of f alone. The universal law (5) eliminates the time variable.

The numbers of bond-breaking events are often reported as functions of time and applied force [1–5]. Such data correspond to the probability density $p(f,t)$ that in the case of time-independent force is related to the probability $P(f,t)$ by $p(f,t) \equiv -\partial P(f,t)/\partial t = \nu(f)\exp[-\nu(f)t]$. The probability density obeys the following universal law:

$$\frac{\ln[p(f,t_0)/p(f,t)]}{t-t_0} = \nu(f), \quad (6)$$

where $t_0 \neq t$ in the first term is some reference time. In the limit of $t \to t_0$ the relationship becomes

$$-\frac{\partial p(f,t)/\partial t}{p(f,t)} = \nu(f). \quad (7)$$

The time derivative of the probability density divided by the density itself is independent of time.

The ratio of the probability density to the probability is also time independent, generating the well-known [25] and useful universal relationship

$$p(f,t)/P(f,t) = \nu(f). \quad (8)$$

The variety of representations of the time-dependent experimental data provided by the above expressions for the constant unbinding force is universally mapped onto the time-independent bond lifetime $\nu(f)$.

B. The jump-ramp scenario

The so-called jump-ramp pulling scenario [5,6] where the force is first rapidly increased to the jump force f_0 and then is linearly ramped with the ramp rate r

$$f(t) = rt + f_0, \quad (9)$$

provides an alternative probe of biological adhesion. The bond-survival probability (4) becomes a function of three variables t, r, f_0. The experimental data are commonly given as a function of force rather than time using the f, r, f_0 variables [5,6]. The linear relationship (9) between t and f allows for a straightforward transformation between the two representations. In the force representation the bond-survival probability is

$$P(f,r;f_0) = \exp\left(-r^{-1}\int_{f_0}^{f} \nu(f')df'\right), \quad (10)$$

and the probability density is equal to

$$p(f,r;f_0) \equiv -\partial P(f,r;f_0)/\partial f = r^{-1}\nu(f)P(f,r;f_0). \quad (11)$$

The following universal law follows from Eqs. (10) and (11):

$$rp(f,r;f_0)/P(f,r;f_0) = \nu(f), \quad f \geqslant f_0. \quad (12)$$

Remarkably, the ratio of the bond-survival probability density to the probability is independent of both the ramp rate and jump force. Moreover, it is equal to the inverse bond lifetime for the constant force regime, Eq. (3).

III. UNIVERSAL REPRESENTATIONS FOR THE EXPONENTIAL FORCE DEPENDENCE OF THE RATE CONSTANT

The general universal laws (5)–(8) and (12) hold for an arbitrary dependence of the rate constants on the force. Detailed universal relationships can be derived assuming the most commonly used exponential force dependence introduced by Bell [16]:

$$k_{1s} = k_{1s}^0 \exp(x_{1s}f/k_BT), \quad k_{1c} = k_{1c}^0 \exp(-x_{1c}f/k_BT) \quad (13)$$

with the focus on the two-pathway model [22–24] of the catch-slip transition, Eq. (3). Here, k_B is the Boltzmann constant and T is temperature. The constants k_{1s}^0 and k_{1c}^0 are the

rates at zero force, and x_{1s} and x_{1c} are the distances between the bound-state minimum and the corresponding barrier maxima. The opposite signs in the exponents for the slip and catch pathways are essential and describe the increased rate of escape along the slip pathway and decreased rate of escape along the catch pathway under the action of the force. Within a well-defined parameter range [22–24] the catch-slip bond lifetime first grows and then decreases with increasing force. The two-pathway model was developed to represent the experiments using a minimal number of parameters compared to the alternative descriptions [5,26]. The model showed fine agreement with the experimental data for both constant and time-dependent pulling-force regimes as well as for monomeric and dimeric binding [22,23].

A. Universal relationships for the bond-survival probability

The bond-survival probability (10) for the jump-ramp scenario (9) can be expressed analytically within the two-pathway catch-slip model, Eqs. (3) and (13), as

$$P(f,r;f_0) = \exp[-k_BT \cdot g(f,f_0)/r], \quad f \geqslant f_0, \tag{14}$$

where

$$g(f,f_0) = \varphi(f) - \varphi(f_0),$$

$$\varphi(f) = \frac{k_{1s}^0}{x_{1s}} \exp\left(\frac{x_{1s}f}{k_BT}\right) - \frac{k_{1c}^0}{x_{1c}} \exp\left(\frac{-x_{1c}f}{k_BT}\right). \tag{15}$$

Rewritten in the form

$$-\frac{r}{k_BT} \ln P(f,r;f_0) = g(f,f_0), \tag{16}$$

Eq. (14) attains the structure of Eq. (5). Since the right-hand side of Eq. (16) contains no r, the combination of the experimental data expressed by the left-hand side is also independent of r. Equation (16) maps the data for different ramp rates onto a single universal curve.

A limited version of Eq. (16) for $f_0=0$ and $k_{1c}^0=0$ describing only the slip bond was considered in [21]. Reference [27] used the special case of Eq. (12) with $f_0=0$ in order to reconstruct the bond-lifetime for the constant force scenario from the time-dependent force measurements.

A further universal relationship that eliminates two of the three variables follows from the specific form of $g(f,f_0)$, Eq. (15). Taking the difference of Eq. (16) evaluated for two arbitrary sets of jump force and ramp rate (r_1,f_{01}) and (r_2,f_{02}) gives

$$\frac{1}{k_BT}[r_2 \ln P(f,r_2,f_{02}) - r_1 \ln P(f,r_1,f_{01})] = \varphi(f_{02}) - \varphi(f_{01}). \tag{17}$$

The left-hand side of the above equation is independent of both r and f, and is defined for $f \geqslant \max(f_{01},f_{02})$. The following useful corollaries follow from Eq. (17):

$$\frac{r}{k_BT} \ln[P(f,r,f_{02})/P(f,r,f_{01})] = \varphi(f_{02}) - \varphi(f_{01}), \tag{17a}$$

if $r_1=r_2$, and

$$P(f,r_2,f_0)^{r_2}/P(f,r_1,f_0)^{r_1} = 1, \tag{17b}$$

if $f_{01}=f_{02}$.

B. Universal relationships for the bond-survival probability density

The probability density for the jump-ramp regime is linearly related to the probability, Eq. (11). Therefore, it follows that the universal law (17a) can be expressed in terms of the probability density simply by replacing P with p.

Equation (11) in combination with Eq. (14) leads to another useful universal relationship for the probability-density:

$$\frac{rr_0}{k_BT(r-r_0)} \ln\left[\frac{rp(f,r;f_0)}{r_0p(f,r_0;f_0)}\right] = g(f,f_0), \tag{18}$$

where $r_0 \neq r$ is an arbitrary reference ramp rate. In the limit of $r \to r_0$ Eq. (18) transforms into

$$\frac{r^2}{k_BT}\left[\frac{1}{r} + \frac{1}{p(f,r;f_0)}\frac{\partial p(f,r;f_0)}{\partial r}\right] = g(f,f_0). \tag{19}$$

The combinations of the experimentally measurable quantities expressed using the probability density by the left-hand sides of the universal relationships (18) and (19) should be independent of r.

The bond lifetime can be easily reconstructed using the following universal law expressed using probability densities for two different values of r:

$$\sqrt[(r_1-r_2)]{\frac{[r_1p(f,r_1,f_{01})]^{r_1}}{[r_2p(f,r_2,f_{02})]^{r_2}}} = \nu(f)\exp\left(k_BT\frac{\varphi(f_{01}) - \varphi(f_{02})}{r_1 - r_2}\right). \tag{20}$$

This relationship follows from Eqs. (11), (14), and (15). The left-hand side contains a combination of experimental quantities only. The right-hand side gives the inverse lifetime $\nu(f)$ multiplied by a constant, which disappears if $f_{01}=f_{02}$.

C. The slip-bond limit

As pointed out in our earlier work [23], the catch features of the catch-slip bond manifest themselves in the low-force region of the bond-survival probability density. The high-force region reveals the properties of the slip component. In particular, if the maximum of the probability density is located in the high-force region, the force f_m at which the maximum occurs is well described by approximating $k_{1c}^0=0$. The resulting expression for f_m as a function of r is well known:

$$f_m = \frac{T}{x_{1s}} \ln \frac{rx_{1s}}{k_BTk_{1s}^0}. \tag{21}$$

Additional information about the receptor-ligand interaction can be obtained by investigating the magnitude of the maximum $p_m(r)$ as a function of the ramp rate r. The $k_{1c}^0=0$ approximation applied to Eqs. (11), (14), and (21) gives

$$p_m(r) = \frac{x_{1s}}{k_B T} \exp\left(\frac{k_B T k_{1s}^0}{r x_{1s}} - 1 \right). \quad (22)$$

Equation (22) shows that as r decreases, the maximum magnitude of the probability density rapidly grows. Since the probability-density distribution is normalized to 1, the increase of its maximum value must be accompanied by the corresponding decrease in its width. Thus, low ramp rates give anomalously narrow probability-density distributions. The opposite case of $r \to \infty$ leads to the limit $p_m(r \to \infty) = x_{1s}/ek_BT$, where e is the base of natural logarithm. The limiting value of the probability-density maximum in this case immediately gives the slip-barrier width x_{1s}. Having data for different ramp rates, one can use the universal relationship

$$\frac{r_1 r_2}{r_2 - r_1} \ln \frac{p_m(r_1)}{p_m(r_2)} = \frac{k_B T k_{1s}^0}{x_{1s}}, \quad (23)$$

which follows from Eq. (22). The left-hand side of Eq. (23) defines a function of the experimentally measurable characteristics. The function is universal for any choice of r_1 and r_2.

IV. DEMONSTRATION OF THE UNIVERSAL LAWS WITH EXPERIMENTAL DATA

The universal relationships derived above allow us to represent the data obtained under a variety of experimental conditions in a compact form, as demonstrated below with the monomeric P-selectin/sPSGL-1 [3,5] catch-slip bond, dimeric P-selectin/PSGL-1 catch-slip bond [1,3], and the E-selectin/sialyl Lewis^x antigen slip-bond [28].

A. The constant force regime

The universal relationship (5) for the constant force regime directly applies to the experimental data of [1,3], which reports the number of bond-breaking events $N(t,f)$ observed over the period of time greater or equal t under the pulling force f. The probability in Eq. (5) corresponds to the normalized number of the bond-breaking events $N(t,f)/N(0,f)$. According to (5) the logarithm of the bond-survival probability divided by time should depend only on force. The mapping is illustrated in Fig. 1(a) using the data of Fig. 3(d) of [3] for the P-selectin/sPSGL-1 complex, which forms a monomeric receptor-ligand bond. Fixing the value of the force, the left-hand side of Eq. (5) was computed for several points in time, as represented by the red circles, which cluster around a single point on the plot. The solid line gives $\nu(f)$ predicted by the double-exponential function (3) and (13) within the two-pathway model [22–24] using the parameters found for the constant force regime, line 2 of Table 1 in [22]: $k_{1s}^0 = 0.25 \pm 0.05\ s^{-1}$, $x_{1s} = 5.1 \pm 0.5$ Å, $k_{1c}^0 = 120 \pm 55\ s^{-1}$, $x_{1c} = 21.7 \pm 2.4$ Å. The corresponding results for the dimeric P-selectin/PSGL-1 complex are shown in Fig. 1(b). The right-hand side of Eq. (5) was computed using the above set of model parameters and Eq. 18 of [22], which relates the lifetimes of the monomeric and dimeric bonds. The red circles were generated using the left-hand side of Eq. (5) from the experimental data from Fig. 3(e) of [3] obtained with atomic force microscopy. The blue triangles represent the experimental data from Fig. 4(a) of [1] obtained with shear-stress experiments. Remarkably, the universal law (5) for the inverse bond lifetime is confirmed by the data taken from the publications that used different types of experiments and experimental setups.

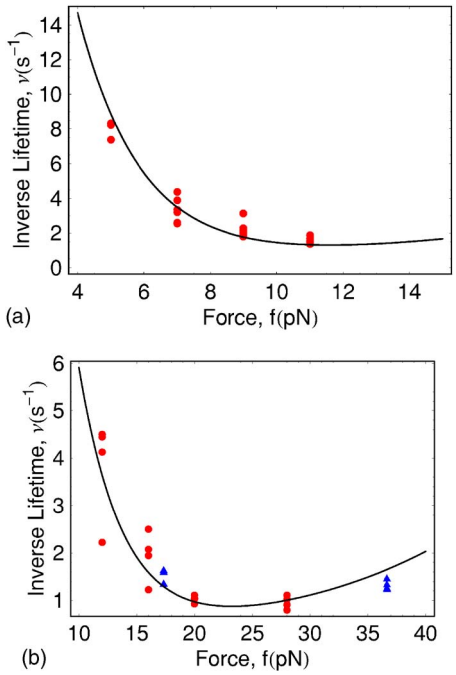

FIG. 1. (Color online) Universal representation of the constant force experiments, Eq. (5), which eliminate the time dependence of the data. The solid lines correspond to the right-hand side of Eq. (5) calculated using Eqs. (3) and (13) for the two-pathway model parameters reported in [22] (second line of Table 1). The circles give experimental data represented with the left-hand side of Eq. (5). The clusters of circles were obtained by selecting several times from the lines in Fig. 3 of [3] and Fig. 4(a) of [1], which show the data for fixed force values. (a) Monomeric bond in the P-selectin/sPSGL-1 complex. The experimental data are taken from Fig. 3(d) of [3] for forces equal to $f=5$, 7, 9, and 11 pN. (b) Dimeric bond in the P-selectin/PSGL-1 complex. The lifetime of the dimeric bond is related to the lifetime of the monomeric bond via Eq. (18) of [22]. The red circles represent experimental data from Fig. 3(e) of [3] for $f=12$, 16, 20, and 28 pN. The blue triangles correspond to the experimental data from Fig. 4(a) of [1] for $f=17.3$ and 36.6 pN.

B. The jump-ramp regime

Figures 2–4 consider the jump-ramp regime, Eq. (9). The force histograms presented in Fig. 2 of [5] were normalized to obtain the probability densities $p(f)$ and integrated to derive the probabilities $P(f) = \int_f^\infty p(f')df'$. Figure 2 illustrates the universal laws (16) and (18). The red triangles and blue squares were obtained using the left-hand side of Eq. (16) based on the data of Fig. 2B ($r = 210pN/s$) and Fig. 2C ($r = 1400pN/s$) of [5], respectively. The data from both figures were taken to generate the green stars using the left-hand side of Eq. (18). The solid line gives the functional dependence of $g(f,f_0)$ on f using the parameters of [22] obtained

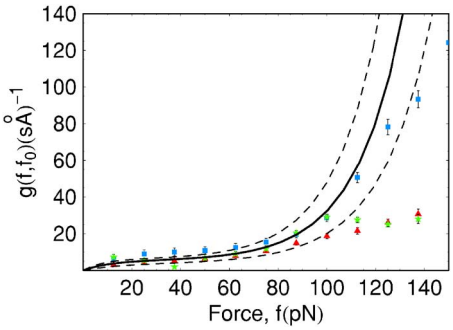

FIG. 2. (Color online) Universal representation of the jump-ramp experiments, Eqs. (16) and (18), which eliminate the ramp-rate dependence of the data. Experimental errors are indicated. The solid line represents the right-hand side of Eqs. (16) and (18) calculated for the two-pathway model parameters reported in [22] (third line of Table 1). The dashed lines estimate the error and are generated using all upper and all lower bounds of these parameters. The red triangles and blue squares are obtained using the left-hand side of Eq. (16) for the experimental data of Fig. 2B and Fig. 2C, respectively, published in [5]. The green stars are obtained by combining both sets of data from these figures, as prescribed by the left-hand side of Eq. (18).

for the jump-ramp regime (line 3 of Table 1): $k_{1s}^0 = 0.34 \pm 0.09\ s^{-1}$, $x_{1s} = 2.1 \pm 0.1$ Å, $k_{1c}^0 = 20 \pm 10\ s^{-1}$, $x_{1c} = 3.8 \pm 1.1$ Å. The dashed lines estimate the error and were generated using all upper and all lower bounds of these parameters. In all cases $f_0 = 0$. The experimental results closely follow the theory up to force values around 100 pN. The possible sources of the deviations between the left- and right-hand sides of the universal relationships (16) and (18) for $f > 100$ pN are discussed below in Sec. IV C.

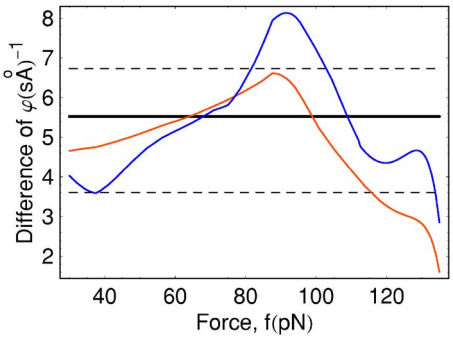

FIG. 3. (Color online) Demonstration of the universal law (17a), which creates a representation of the jump-ramp data that are independent of both force and ramp rate. The thick black line represents the difference of the φ functions, which are present in the right-hand side of Eq. (17a) and are defined in Eq. (15). The calculation is done for the two-pathway model parameters reported in [22] (third line of Table 1). The dashed lines estimate the error and are generated using the upper and lower bounds on these parameters. The red (lighter gray) and blue (darker gray) lines correspond to the probability and probability density, respectively. These lines are generated with the left-hand side of Eq. (17a) using the experimental data of Figs. 2B and E of [5]. Since the probability and probability density are linearly related, Eq. (11), the universal relationship (17a) applies to both of them.

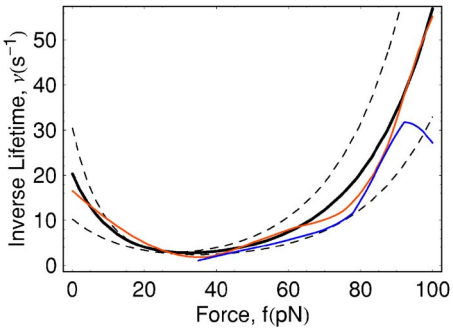

FIG. 4. (Color online) Demonstration of the universal law (20), which arranges the jump-ramp experimental results in such functional form that gives the bond dissociation rate $\nu(f)$. The latter is important for both the constant force and jump-ramp regimes. The thick black solid line shows $\nu(f)$ obtained using Eqs. (3) and (13) for the two-pathway model parameters reported in [22] (third line of Table 1). The dashed lines estimate the error and are generated using the upper and lower bounds of these parameters. The dissociation rate $\nu(f)$ determines the right-hand side of Eq. (20). The left-hand side of Eq. (20) is represented by the red (lighter gray) and blue (darker gray) lines, which are computed using the experimental data from Figs. 2B and C and Figs. 2E and F, respectively, published in [5]. The exponential factor multiplying $\nu(f)$ in the right-hand side of Eq. (20) equals exactly 1 for the red line and 1.01 for the blue line.

Figure 3 demonstrates the universal representation (17a) that eliminates two of the three variables. The difference of functions φ entering the right-hand side of Eq. (17a) is independent of both ramp rate r and rupture force f. The difference was computed using the above values of the parameters and the jump forces $f_{01} = 0$ and $f_{02} = 30$ pN. As in Fig. 2 and Fig. 4, the dashed lines estimate the errors and were computed using all upper and all lower bounds of the parameters. The experimental data were taken from Figs. 2B,E of Ref. [5] for the ramp rate $r = 210 pN/s$. Since the force values used to bin the experimental histograms are not exactly the same in the two figures, the experimental data were interpolated. The red and blue lines are for probability and probability-density, respectively, and were calculated using the left-hand-side of Eq. (17a), which applies to both functions.

C. Relationship between the constant force and jump-ramp regimes

Figure 4 demonstrates the universal representation (20). It allows one to reconstruct the functional dependence of the inverse bond lifetime on force (right-hand side of the equation) based on the experimental observables (left-hand side of the equation). The thick black line gives the theoretical values of $\nu(f)$ computed with Eqs. (3) and (13) using the same values of the model parameters as in Figs. 2 and 3. The dashed lines estimate the errors based on the parameter uncertainties. The red and blue curves correspond to the left-hand side of Eq. (20). The red curve is based on the data of Fig. 2B ($r_2 = 210$ pN/s, $f_{02} = 0$ pN) and Fig. 2C ($r_1 = 1400$ pN/s, $f_{01} = 0$ pN) of [5]. The blue curve corresponds to the data of Fig. 2E ($r_2 = 210$ pN/s, $f_{02} = 30$ pN) and Fig. 2F

(r_1=1400 pN/s, f_{01}=35 pN) of [5]. Note that bond-survival probability density is defined only for $f > f_0$. Therefore, the blue curve starts at 35 pN. Also note that the exponent multiplying $\nu(f)$ in the right-hand side of Eq. (20) is exactly one for the red curve and is 1.01 for the blue curve.

The data shown in Figs. 2–4 are in good agreement with the theoretical relationships (16), (17a), (18), and (20) up to forces around 100 pN. The deviations seen with $f > 100$ pN can be explained with the comment in the caption of Fig. 2 of [5]: The tails in the experimental histograms at high forces may be due to the small probability of forming two bonds between the microspheres covered with P-selectin and sPSGL-1. Even if the fraction of microspheres connected by two or more P-selectin/sPSGL-1 complexes is small, their effect on the bond-survival probability and probability density grows with increasing force. At large forces most of the single connections dissociate rapidly and the experimental data become dominated by multiple connections. The theoretical results shown in Figs. 2–4 were obtained for a single P-selectin/sPSGL-1 complex for all forces. The deviations may also arise due to the assumption that the bond-dissociation rate constant depends on the force exponentially, which is strictly valid only for time-independent potentials. Alternatively, the deviations may indicate that the system is too complex to be described by the model [22–24] and may require more advanced descriptions, such as those developed in [5,26,27,29].

D. The slip-bond limit

Finally, the relationships (22) and (23) are illustrated with the experimental data of [28] that reported force-distribution histograms for the E-selectin/sialyl Lewis^x complex measured over a wide range of r values (see Fig. 8 of [28]). The complex exhibited only the slip behavior and, therefore, Eqs. (21)–(23) should be applicable to all data. The experimental results confirm the conclusion following from Eq. (22) that the maximum value of the bond-survival probability density dramatically grows with decreasing r and approaches a finite limit for large $r \gg r_0 = k_B T k_{1s}^0 / x_{1s}$. Using the parameters reported in [28], $k_{1s}^0 = 2.2\ \mathrm{s}^{-1}$, $x_{1s} = 0.16$ Å, we obtain $r_0 = 564$ pN/s. This agrees with the experimental fact that the probability-density maximum has reached its limit by $r \approx 5000$ pN/s. In order to demonstrate the universal relationship (23) we note that the right-hand side of (23) equals r_0. Choosing $r_1 = 285$ pN/s, $r_2 = 3600$ pN/s, the left-hand side becomes 534 pN/s. For $r_1 = 650$ pN/s, $r_2 = 1800$ pN/s, the left-hand side is 676 pN/s. Both values are close to $r_0 = 564$ pN/s. Given that the experiments [28] were tuned primarily to measure the change in the position f_m of the probability-density maximum as a function of r and not its absolute magnitude p_m that enters Eq. (23), the above results provide solid support for this universal relationship.

V. CONCLUSIONS

We have established both general (5)–(8) and (12) and detailed (16)–(23) universal laws for the probability and probability-density distribution functions. The general laws follow from the kinetic equations describing bond dissociation and are valid for an arbitrary force dependence of the rate constants. The detailed laws are developed assuming the most common exponential force dependence of the rate constant. Both the catch-slip bond and its slip-bond limit have been investigated. Particular consideration has been given to the now standard constant and jump-ramp force experiments.

The derived relationships contain experimental observables on one side of the equation and model parameters on the other side, thereby creating universal correspondence between the experimental data and theoretical results. Standard experimental functions that depend of several variables have been combined into representations that reduce the number of variables. Multiple observables have been mapped onto universal functions that directly relate data sets obtained with different force protocols. Both general (5)–(8) and (12) and detailed (16)–(23) relationships have been illustrated with the monomeric P-selectin/sPSGL-1 catch-slip bond, the dimeric P-selectin/PSGL-1 catch-slip bonds, and the E-selectin/sialyl Lewis^x slip-bond.

Application of the universal relationships to the selectin bonds uncovered new insights into the physics of these systems. The deviations from the universal relationships at forces above 100 pN suggest that the high force data may include significant contributions from multiple bonds. Alternatively, the discrepancy may arise because the commonly used models are not adequate in the high force regime. More advanced descriptions may require additional bound states and dissociation pathways [5,26] or explicit treatment of the linker connecting the ligand to the atomic force microscopy tip [30]. Since the constant-force and jump-ramp results are directly related, e.g., Eq. (12), they should be described by the same set of model parameters. However, this is not the case for the P-selectin bond, see Table 1 of [22], indicating that either the experimental data were obtained under different conditions or the model is too simplistic. For instance, one can question whether the exponential form of the rate-constant, Eq. (13), can be applied in the case of a time-dependent force.

Other physical conclusions follow from the above analysis independently of the system. For sufficiently large forces and force loading rates, biological bonds behave as slip bonds. In order to characterize the more intricate details of biological binding, such as the catch-binding, one should use small forces and force loading rates. Some of the slip-bond properties, such as the maximum value of the bond-survival probability density, approach limits with increasing loading rate. Exceeding the limiting loading-rate carries little additional information about the bond. The universal relationships derived above suggest which ranges of the experimentally controllable variables are most useful for bond characterization.

Most experimental data are presented in the form of bond-survival probability density, as stipulated by the experimental procedure. It is straightforward to convert probability density to probability. The universal relationships formulated in the probability language provide additional tests for experimental results. The mapping of the experimental data obtained within different regimes onto the same curve greatly facilitates data fitting. Since the mapping increases the data den-

sity, the number of measurements required to reduce the experimental error to a desired quality can be substantially reduced.

Various models and experimental regimes allow different analytical levels of analysis. On the one hand, the ability to derive the universal relationships creates a useful criterion for differentiating between the models of the same level of complexity. On the other hand, the ease of deriving the universal laws can suggest new experiments or help to choose between several experimental possibilities. For instance, it is particularly valuable to investigate the properties of the catch-slip bond under the action of a periodic force, since *in vivo* the bond functions in a pulsed blood flow [24]. Alternative pulling regimes, such as a continuous cosine function or a piecewise sawtooth function, create different possibilities for analytical treatment. Since universal laws provide additional benefits in the data analysis and create new physical insights, the regime that is best suited for deriving such laws is preferable experimentally.

To recapitulate, the derived universal laws allow one to test the internal consistency of experimental data and theoretical models, to hypothesize on the discrepancies between theory and experiment, to reduce the error bars and improve the quality of fits, and, generally, to facilitate the dynamic force spectroscopy studies of biological adhesion.

ACKNOWLEDGMENTS

The authors are grateful to Evgeni Sokurenko and Wendy Thomas for fruitful discussions and thank Kim Gunnerson for comments on the manuscript. The financial support of DOE Grant No. DE-FG02-05ER15755, ACS PRF Grant No. 41436-AC6 and NIH Bioengineering Research Partnership Grant R01 AI050940 is much appreciated.

[1] R. Alon, D. A. Hammer, and T. A. Springer, Nature (London) **374**, 539 (1995).
[2] E. Finger, K. Puri, R. Alon, M. Lawrence, U. von Andrian, and T. Springer, Nature (London) **379**, 266 (1996).
[3] B. T. Marshall, M. Long, J. W. Piper, T. Yago, R. P. McEver, and C. Zhu, Nature (London) **423**, 190 (2003).
[4] K. K. Sarangapani, T. Yago, A. G. Klopocki, M. B. Lawrence, C. B. Fieger, S. D. Rosen, R. P. McEver, and C. Zhu, J. Biol. Chem. **279**, 2291 (2004).
[5] E. Evans, A. Leung, V. Heinrich, and H. Zhu, Proc. Natl. Acad. Sci. U.S.A. **101**, 11281 (2004).
[6] E. Evans, Annu. Rev. Biophys. Biomol. Struct. **30**, 105 (2001).
[7] C. Bustamante, Z. Bryant, and S. B. Smith, Nature (London) **421**, 423 (2003).
[8] F. Mohammad-Rafiee and R. Golestanian, Phys. Rev. Lett. **94**, 238102 (2005).
[9] H. B. Li and J. M. Fernandez, Science **303**, 1674 (2004).
[10] L. P. Silva, Curent Protein & Peptide Science **6**, 387 (2005).
[11] O. Gliko, I. Reviakine, and P. G. Vekilov, Phys. Rev. Lett. **90**, 225503 (2003).
[12] A. E. Filippov, J. Klafter, and M. Urbakh, Phys. Rev. Lett. **92**, 135503 (2004).
[13] W. E. Thomas, E. Trintchina, M. Forero, V. Vogel, E. V. Sokurenko, Cell **109**, 913 (2002).
[14] M. Forero, W. E. Thomas, C. Bland, L. M. Nilsson, E. V. Sokurenko, and V. Vogel, Nano Lett. **4**, 1593 (2004).
[15] M. Dembo, D. C. Torney, K. Saxman, and D. A. Hammer, Proc. R. Soc. London, Ser. B **234**, 55 (1988).
[16] G. I. Bell, Science **200**, 618 (1978).
[17] U. Seifert, Phys. Rev. Lett. **84**, 2750 (2000).
[18] B. Heymann and H. Grubmuller, Phys. Rev. Lett. **84**, 6126 (2000).
[19] T. Erdmann and U. S. Schwarz, Phys. Rev. Lett. **92**, 108102 (2004).
[20] G. Hummer and A. Szabo, Acc. Chem. Res. **38**, 504 (2005).
[21] M. Evstigneev and P. Reimann, Phys. Rev. E **68**, 045103(R) (2003).
[22] Y. V. Pereverzev, O. V. Prezhdo, M. Forero, E. V. Sokurenko, and W. E. Thomas, Biophys. J. **89**, 1446 (2005).
[23] Y. V. Pereverzev, O. V. Prezhdo, W. E. Thomas, and E. V. Sokurenko, Phys. Rev. E **72**, 010903 (2005).
[24] Y. V. Pereverzev and O. V. Prezhdo Biophys. J. **91**, L19 (2006).
[25] P. Beckmann, *Probability in Communication Engineering* (Harcourt, Brace & World, New York, 1967).
[26] V. Barsegov and D. Thirumalai, Proc. Natl. Acad. Sci. U.S.A. **102**, 1835 (2005).
[27] B. T. Marshall, K. K. Sarangapani, J. Lou, R. P. McEver, and C. Zhu, Biophys. J. **88**, 1458 (2005).
[28] D. F. Tees, R. E. Waugh, and D. A. Hammer, Biophys. J. **80**, 668 (2001).
[29] Y. V. Pereverzev and O. V. Prezhdo Phys. Rev. E **73**, 050902 (2006).
[30] H. Qian and B. E. Shapiro, Proteins: Struct., Funct., Genet. **37**, 576 (1999).